Biosensors and Bioelectronics 72 (2015) 237–246

Contents lists available at ScienceDirect

Biosensors and Bioelectronics

journal homepage: www.elsevier.com/locate/bios

A simultaneous electrochemical multianalyte immunoassay of high sensitivity C-reactive protein and soluble CD40 ligand based on reduced graphene oxide-tetraethylene pentamine that directly adsorb metal ions as labels

Guolin Yuan [1], Chao Yu [1], Chunyong Xia, Liuliu Gao, Wailan Xu, Wenjuan Li, Junlin He *

Institute of Life Science and School of Public Health, Chongqing Medical University, Chongqing 400016, PR China

ARTICLE INFO

Article history:
Received 28 February 2015
Received in revised form
9 April 2015
Accepted 27 April 2015
Available online 30 April 2015

Keywords:
Simultaneous detection
Reduced graphene oxide-tetraethylene pentamine
Metal ion labels
High sensitive C-reactive protein
Soluble CD40 ligand

A simplified electrochemical multianalyte immunosensor for the simultaneous detection of high sensitivity C-reactive protein (hsCRP) and soluble CD40 ligand (sCD40L) that uses reduced graphene oxide-tetraethylene pentamine (rGO-TEPA) that directly adsorbs metal ions as labels is reported. rGO-TEPA contains a large number of amino groups and has excellent conductivity, making it an ideal template for the loading of Pb^{2+} and Cu^{2+}, which greatly amplifies the detection signals. The signals could be directly detected in a single run through differential pulse voltammetry (DPV), and each biorecognition event produces a distinct voltammetric peak. The position and size of each peak reflects the identity and the level of the corresponding antigen. Primarily designed for an application in a sandwich-type immunoassay based on Pb^{2+} and Cu^{2+} labels, two main challenges are accomplished with the herein presented nanosheets: fabrication of the template and the amination process for Pb^{2+} and Cu^{2+} adsorption. To further improve the analytical performance of the immunosensor, Au@bovine serum albumin (BSA) nanospheres synthesized through a "green" synthesis route were used as a sensor platform, which not only provides a biocompatible microenvironment for the immobilization of antibodies but also amplifies the electrochemical signals. Under optimal conditions, hsCRP and sCD40L could be assayed in the range of 0.05 to 100 ng mL^{-1} with detection limits of 16.7 and 13.1 pg mL^{-1} ($S/N=3$), respectively. The assay results on clinical serum samples with the proposed immunosensor were in acceptable agreement with those using the standard single-analyte test of the enzyme-linked immunosorbent assay (ELISA). This novel immunosensing system provides a simple, sensitive and low-cost approach for a multianalyte immunoassay.

1. Introduction

Cardiovascular disease (CVD) was listed as the primary cause of death globally by the World Health Organization (WHO), accounting for approximately 18 million deaths annually (Fakanya and Tothill, 2014). Currently, the standard 12-lead electrocardiogram (ECG) is the single best test to identify patients with acute CVD (Gibler et al., 2005). However, it is necessary to develop complementary chemical assay methods for the detection of acute myocardial infarction (AMI). Biomarker detection is the best method to identify patients following the ECG (Willcox et al., 2004). Several biomarkers are associated with an increased risk of cardiovascular disease, including high sensitivity C-reactive protein (hsCRP) and Soluble CD40 ligand (sCD40L) (Guldiken et al., 2011). hsCRP, a precursor to cardiovascular disease, is very sensitive to AMI (Babakhanian et al., 2015; Dieset et al., 2012; Vashist et al., 2015). sCD40L is a ligand of the glycoprotein Πb-Ша receptor and is involved in thrombus stabilization and platelet activation. (Unek et al., 2010). There is an evidence that the sCD40L level is a strong predictor of cardiovascular risk (Erturan et al., 2014; Unek et al., 2010; Zhang et al., 2014a). Biomarkers have been proven to work better as a panel because no single biomarker is specific and sensitive enough to meet the strict diagnostic criteria of clinical diagnosis (Wu et al., 2014). In addition, different biomarkers are released into the blood stream at different pathophysiological stages of CVD and return back to their baseline levels after some time (Apple, 2007; Willcox et al., 2004). Therefore, simultaneous detection of two compounds is particularly important. Recently, the development of an immunoassay that enables the simultaneous determination of biomarkers has attracted extensive interest (Bai et al., 2012; Jia et al., 2014; Li et al., 2014, 2013; Liu et al., 2012). Among various measurement techniques, electrochemical immunoassays are an ideal strategy due to their

* Corresponding author. Fax: +86 23 68486294.
E-mail address: hejunlin_11@aliyun.com (J. He).
[1] Chao Yu and Guolin Yuan contributed equally to this work.

http://dx.doi.org/10.1016/j.bios.2015.04.088
0956-5663/

advantages of portability, high sensitivity, rapid analysis, and low cost (Xu et al., 2014). To the best of our knowledge, there is no report on the simultaneous electrochemical detection of hsCRP and sCD40L yet. It is worth mentioning that their combined measurement may not only increase the sensitivity of the risk prediction but also provide new cardiac markers to replace cardiac enzymes for the clinical diagnosis and risk evaluation of cardiovascular events. Thus, we intend to fabricate an electrochemical immunosensor to simultaneously detect hsCRP and sCD40L in human serum.

For the development of a multiplex electrochemical immunoassay, the fabrication of label-anchored secondary antibodies for generating signals is of great importance in improving the sensitivity of the immunosensor. Numerous signal tags have been used for signal amplification such as enzymes (Zhao et al., 2014), metal nanoparticles and quantum dots (QDs) (Feng et al., 2012b). The easy inactivation and costly preparation and purification processes of enzymes restrict their applications (Zhao et al., 2014). Metal nanoparticles and QDs require a complicated and tedious preparation process (Feng et al., 2012b), as well as a time-consuming acid dissolution step and metal preconcentration before the electrochemical detection. As a result, great efforts have been made to fabricate novel labels for metallo-immuoassays to simplify the detection steps. In previous studies, Cd^{2+}-functionalised titanium phosphate nanoparticles (Feng et al., 2012b) and metal ion (Cd^{2+}, Zn^{2+})-functionalised titanium phosphate nanospheres (Feng et al., 2012a) were used as labels for electrochemical immunoassays based on the ion-exchange capability of titanium phosphate nanoparticles. However, the fabrication of the template for metal ion immobilization is a time-consuming job. Amino-capped nanomaterials showed good adsorption properties for Pd^{2+}, Ni^{2+}, Cd^{2+}, $Ag+$ and Cu^{2+} (Xu et al., 2014), and therefore, they provided another strategy for the immobilization of metal ions on immunosensor probes (Xu et al., 2014). Notably, to realize the adsorption of metal ions for amplification, the template should qualify both amino-groups and conductivity. Amino-group functionalised mesoporous Fe_3O_4 loaded with Pb^{2+} and Cd^{2+} (Zhang et al., 2014b), Cd^{2+}-functionalized nanoporous TiO_2 (Zhao et al., 2014), and amino-capped PtPNPs complexed with Cd^{2+} and Cu^{2+} (Wang et al., 2014) have been reported as labels for the detection of multiplex biomarkers. However, these modification steps are all complicated, owing to the amination process of the template nanomaterials. Ma et al. (2015) utilized metal ions as labels for the assay of proteins, but the modification steps introduced amino-group qualified materials that were nonconductive, which also made the operation procedure time-consuming. Thus, if metal ions (such as Cd^{2+}, Pb^{2+} and Cu^{2+}) could directly conjugate with an amino-group qualified, conductive nanomaterial, the amination process could be eliminated, avoiding the above-mentioned problems.

A novel material, rGO-TEPA (reduced graphene oxide-tetraethylene), which combines reductive graphene oxide (rGO) with tetraethylene pentamine through covalent bonding, has been developed (Wu et al., 2014; Zhang et al., 2014c). This combination possesses the bulk properties of rGO but with improved stability (Guo et al., 2015; Wu et al., 2014, 2015). Most importantly, rGO-TEPA contains a large number of amino groups and has excellent conductivity, which makes it an ideal template for the loading of metal ions. To the best of our knowledge, rGO-TEPA adsorbed metal ions as probes for electrochemical immunoassays have not been reported in the literature. Usage comparison of rGO-TEPA in the electrochemical immunoassay is shown in Table S6. Therefore, to further simplify the routine modification steps, a functionalised rGO nanomaterial, rGO-TEPA, was introduced in the fabrication of a multiplex electrochemical immunosensor.

To further increase the sensitivity for biomarker detection, great efforts have been made toward bio-component immobilization and signal amplification for sandwich-type immunoassays. Therefore, a nanomaterial-based sensor platform with a large surface area and superior conductivity can be used. Au@BSA nanospheres are an ideal nanomaterial owing to their good biocompatibility and excellent conductivity (Cao et al., 2015; Ma et al., 2015). In addition, they can be synthesized through a “green” synthesis route by using the benign reductant ascorbic acid in place of hydrazine monohydrate for the preparation of core–shell nanomaterials (Qu et al., 2013). The resulting unique three-dimensional architecture not only provides a biocompatible microenvironment for the immobilization of antibodies but also amplifies the electrochemical signals.

Herein, we designed a novel and facial sandwich-type immunoassay for the simultaneous detection of hsCRP and sCD40L by employing Au@BSA and rGO-TEPA for dual amplification. The application of Au@BSA not only provided a biocompatible microenvironment for the immobilization of antibody but also accelerated the electron transfer rate to amplify the electrochemical signals. Meanwhile, rGO-TEPA contains a large number of amino groups and has excellent conductivity, which makes it an ideal template for loading numerous metal ions such as Pb^{2+} and Cu^{2+} to form rGO-TEPA-metal ion labels. hsCRP and sCD40L antibodies were conjugated with rGO-TEPA-Pb^{2+} and rGO-TEPA-Cu^{2+} to fabricate anti-hsCRP- rGO-TEPA-Pb^{2+} and anti-sCD40L-rGO-TEPA-Cu^{2+} probes, respectively. The metal ions in the bioconjugates can be detected by differential pulse voltammetry (DPV) without the acid dissolution and preconcentration required by stripping voltammetry, which greatly simplifies the detection steps and reduces the detection time. This proposed strategy exhibited good stability, precision, and reproducibility, suggesting a wide range of potential diagnostic applications.

2. Materials and methods

2.1. Materials and reagents

hsCRP, mouse monoclonal capture anti-bodies (Ab_1) and signal antibodies (Ab_2) of antigen were purchased from Linc-Bio Science Co., Ltd. (Shanghai, China). sCD40L, mouse monoclonal capture anti-bodies (Ab_1) and signal antibodies (Ab_2) of antigen were purchased from Abcam (USA). hsCRP and sCD40L ELISA kits were obtained from Linc-Bio Science Co., Ltd. (Shanghai, China). $HAuCl_4 \cdot 3H_2O$ was obtained from Sigma-Aldrich (St. Louis, USA, www.sigmaaldrich.com). L-ascorbic acid (AA) was bought from Aladdin Ltd. (Shanghai, China). Reduced graphene oxide–tetraethylene pentamin (rGO-TEPA) were purchased from Nanjing XFNANO Materials TECH Co., Ltd. (China). $Pb(NO_3)_2$, $Cu(NO_3)_2$ and Bovine Serum Albumin (BSA), potassium ferricyanide ($K_3Fe(CN)_6$) and potassium ferrocyanide ($K_4Fe(CN)_6$) were purchased from Beijing Chemical Reagents Company (Beijing, China). Glutaraldehyde (GA) was ordered from Sinopharm Chemical Reagent Company Limited (China). Clinical serum samples were obtained from a local hospital and stored at 4 °C. Phosphate buffered solution (PBS) (pH 7.4, 0.1 M) was prepared with NaH_2PO_4 and Na_2HPO_4. HAc/NaAc solutions with different pH values were prepared by mixing the stock solutions of HAc and NaAc. All other reagents were of analytical reagent grade and used without further purification. Ultrapure water (>18.2 MΩ) obtained from a Millipore Mill-Q purification system was used throughout the experiment.

2.2. Apparatus

All electrochemical experiments were carried out on a CHI660D electrochemical workstation (Chenhua Instruments Co., Shanghai, China). Transmission electron microscopy (TEM) investigations were performed on a Hitachi-7500158 (Hitachi Limited, Japan). Scanning electron microscopy (SEM) images were obtained by using a Hitachi S-3000N (Hitachi Limited, Japan). Field emission

scanning electron microscopy (FE-SEM) image was conducted using a Hitachi S4800 (Hitachi Limited, Japan). Energy dispersive X-ray spectroscopy (EDS) was measured using a JEOL JSM-6700F microscope (Japan). Atomic absorption spectroscopy (AAS) was monitored by a Hitachi 180-80 spectrometer. Fourier transform infrared (FT-IR) spectroscopic was recorded on a Nicolet 6700 FT-IR spectrometer (Thermo Nicolet, USA). UV–vis absorption spectrums were recorded using a UV-1800 spectrophotometer (Shimazu, Japan). A conventional three-electrode system was used for all electrochemical measurements: a platinum wire electrode as the counter electrode, a saturated calomel electrode (SCE) as the reference, and the modified glassy carbon electrode (GCE, 4-mm in diameter) as the working electrode.

2.3. Preparation of AU@BSA nanospheres

Au@BSA nanospheres were synthesised according to the literature (Ma et al., 2015) with slight modifications. Five milligrams of BSA was initially dissolved by ultrasonication in 5 mL of Milli-Q water. Then, 2 mL of 1% (w/w) gold chloride solution was dropped into the BSA solution and the mixture was stirred for 5 min, at room temperature. Following that, 5 mg AA was quickly added, and the mixture was allowed to react for 5 min under magnetic stirring. Afterward, the obtained solid product was centrifuged and washed with Milli-Q water and ethanol three times. Finally, the product was stored at 4 °C until use.

2.4. Preparation of Ab_2-rGO-TEPA-metal ion probes

For the absorption of metal ions, 1 mL of rGO-TEPA nanosheets (20 mg mL^{-1}) was dispersed in 17 mL of 10 mM $Pb(NO_3)_2$ and $Cu(NO_3)_2$ aqueous solutions and was stirred at 50 °C for 24 h. Pb^{2+} and Cu^{2+} were separately absorbed on the rGO-TEPA surface by the abundant amino groups of rGO-TEPA. Then, the resultant hybrid nanosheets were recovered by centrifugation and were washed with Milli-Q water three times. The rGO-TEPA-metal ion products were dispersed in 2 mL of Milli-Q water to achieve a dispersion of rGO-TEPA-metal ions with a concentration of 10 mg mL^{-1}.

For the immobilization of Ab_2, 1 mL of the as-prepared rGO-TEPA-metal ion hybrids (2 mg mL^{-1}) was mixed with 1 mL of GA (2.5 wt%) and gently stirred for 1 h at room temperature. Subsequently, 1 mL of

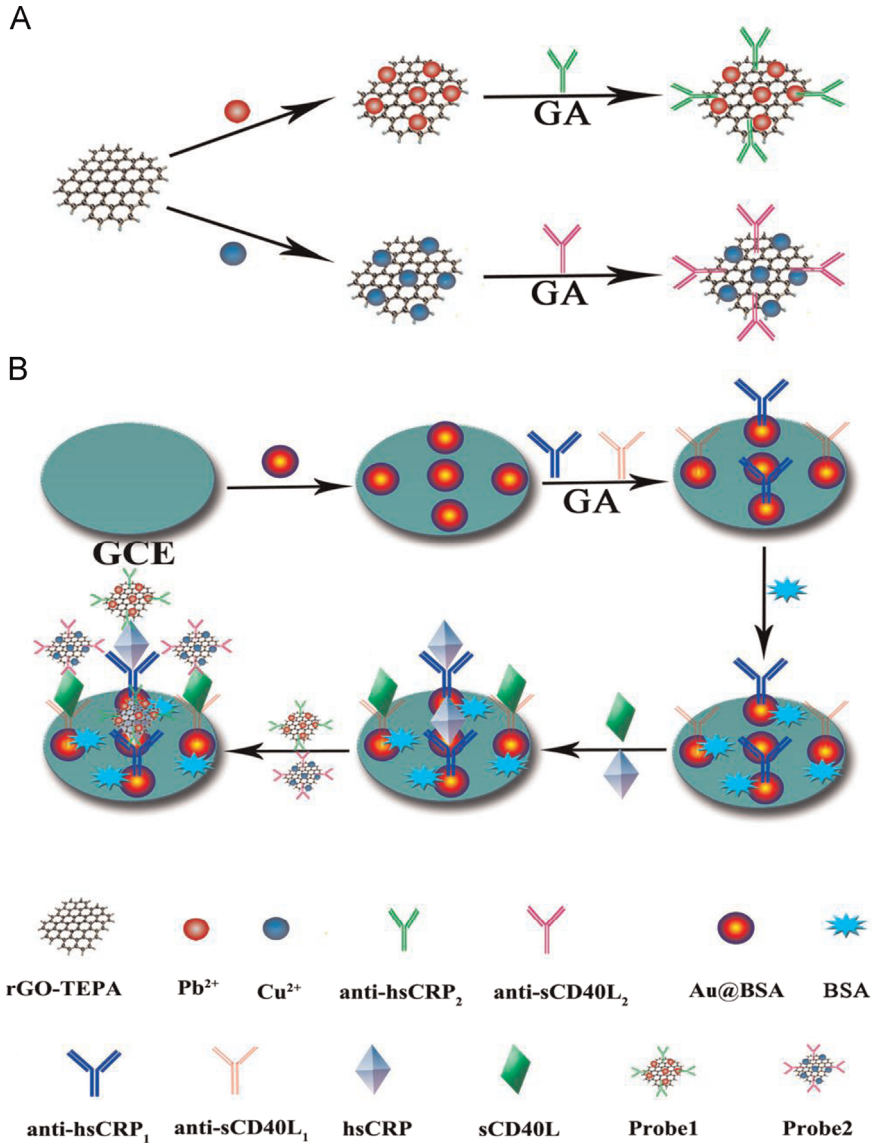

Fig. 1. (A) Preparation procedure of anti-bodies labeled with rGO-TEPA and metal ion hybrids as probes. (B) Schematic illustration of the electrochemical immunoassay protocol.

anti-hsCRP (10 g mL^{-1}) solution was added gently into the rGO-TEPA-Pb^{2+} hybrid and 1 mL of anti-sCD40L (10 g mL^{-1}) solution was added into the rGO-TEPA-Cu^{2+} hybrid, and each was shaken at 4 °C for 12 h. The antibodies were conjugated with the rGO-TEPA-metal ion hybrids through GA cross-linking between the $-NH_2$ of the rGO-TEPA-metal ion hybrids and the $-NH_2$ of the antibodies. The obtained anti-hsCRP-rGO-TEPA-Pb^{2+} and anti-sCD40L-rGO-TEPA-Cu^{2+} were centrifuged and further washed with PBS (0.1 M, pH=7.4) three times and blocked with 1 mL of BSA (1 wt%) for 1 h. After being centrifuged and washed with PBS (0.1 M, pH=7.4), the obtained bioconjugates were resuspended in 1 mL of 0.1 M PBS (pH=7.4) as the assay solution and stored at 4 °C until use. The preparation of the probes is shown in Fig. 1A.

2.5. Fabrication of the immunosensor

The fabrication procedure of the immunosensor is illustrated in Fig. 1B. Prior to use, a glassy carbon electrode (GCE, 4-mm diameter) was polished repeatedly using 0.3- and 0.05-μm alumina slurries followed by thoroughly rinsing with Milli-Q water. After successive sonication in baths of water, absolute alcohol and water again, the electrode was allowed to dry at room temperature. First, 6 μL of Au@BSA (5 mg mL^{-1}) was dropped onto the electrode surface and dried in the air. Subsequently, to cross-link the targeting molecules, 4 μL of GA (2.5 wt%) solution was cast onto the modified electrode surface and incubated for 1 h at room temperature. After the reaction, the electrodes were washed with PBS (pH=7.4) to remove loosely bound chemicals and dried in nitrogen. Afterward, the mixture of hsCRP and sCD40L Ab_1s (6 μL, 10 μg mL^{-1}) was immobilized onto the Au@BSA surface through cross-linking between the aldehyde and amino groups for 12 h at 4 °C, as the biomolecules could retain their bioactivities for a long time at this temperature. After washing with PBS (0.1 M, pH=7.4) to physically remove the antibodies, the modified immunosensor was incubated in a 1 wt% BSA solution for 1 h at 37 °C to eliminate nonspecific binding sites between the analyte and the electrode.

2.6. Measurement procedure

Based on the typical procedure of the sandwich-type immunoassay, 6 μL of the target antigens (hsCRP and sCD40L) solution or serum samples of different concentrations was coated onto the electrodes to form the antigen–antibody immunocomplex, and they were then incubated for 1 h at 37 °C because the immunoreactions could obtain higher efficiencies at this temperature. Subsequently, the electrode was thoroughly washed with PBS (0.1 M, pH=7.4) to remove unbounded target antigens. Finally, 6 μL of the as-prepared bioconjugates was added onto the electrode surface and kept at 37 °C for 1 h to construct a sandwiched immunocomplex based on the principle of highly biospecific recognition between antigens and the corresponding antibodies.

To carry out the electrochemical measurement based on the increase in the response currents of Pb^{2+} and Cu^{2+} in 0.2 M HAc/NaAc (pH=4.5), DPV scans were performed from −1.0 to 0.2 V (vs. SCE) to record the electrochemical responses, which were directly proportional to the concentrations of hsCRP and sCD40L, respectively. Thus, the hsCRP and sCD40L in the serum samples could be determined quantitatively according to the linear relationship.

3. Results and discussion

3.1. Characterizations of AU@BSA nanospheres

The morphology of the Au@BSA nanospheres was characterised by SEM and TEM. Fig. S1A shows the good monodispersity and uniform spherical morphology, with an average size of 500 nm in diameter. Fig. S1B displays a typical TEM image of Au@BSA, which clearly reveals its core–shell structure with a thin layer (BSA) wrapped outside. To further monitor the formation of the Au@BSA nanospheres, EDS characterization was employed to analyze their detailed composition. As shown in Fig. S1C, several intense peaks of Au were observed, suggesting that the Au@BSA had been successfully synthesised. FT-IR was used to characterize Au@BSA, as shown in Fig. S1D. In the spectrum, a broad peak at 3290 cm^{-1} was observed, which was ascribed to the combination of the N–H and O–H stretching of BSA. The broad peaks at 1650 cm^{-1} and 1540 cm^{-1} correspond to the bands of proteins for amide I groups at 1610–1690 cm^{-1} consistent with C=O stretching and amide II groups at 1500–1600 cm^{-1} from a combination of N–H bending and C–N stretching. The characteristic peaks at 1450 cm^{-1} and 1230 cm^{-1} correspond to the bending vibrations of the $-NH_2$ groups in BSA and the stretching vibration of the C–C groups. The results indicate that the primary chemical groups of BSA were maintained and could be used for the immobilization of antibodies.

3.2. Characterization of the metal ion tagged immunosensing probes

Fig. 2(A) and (B) displays the typical SEM and FE-SEM images of rGO-TEPA. It was confirmed that rGO-TEPA has a wrinkled, paper-like structure. The large surface area of rGO-TEPA favors electron transport, while its abundant amino groups encourage Pb^{2+} and Cu^{2+} to absorb on its surface

Figs. 2C and 3A display typical SEM images of the rGO-TEPA-Pb^{2+} and rGO-TEPA-Cu^{2+} hybrids. Their morphologies did not change much, which suggests that the ion absorption process did not destroy the structure of the rGO-TEPA. The presence of Pb^{2+} and Cu^{2+} in the rGO-TEPA-metal ion hybrids was analyzed with EDS, as shown in Figs. 2D and 3B. The signature peaks of C, N, and O were observed in rGO-TEPA, while the presence of Pb^{2+} and Cu^{2+} in the rGO-TEPA-metal ion hybrids was also confirmed. The amounts of Pb^{2+} and Cu^{2+} adsorbed onto rGO-TEPA were further measured using an atomic absorption spectrophotometer (AAS), revealing that 47.97 g of Pb and 21.19 μg of Cu^{2+} were loaded onto 1.0 mg of rGO-TEPA. The rGO-TEPA-metal ion hybrids could then be used as probes for the bioassay.

Figs. 2E and 3C show typical SEM images of the $Ab_{2,1}$-rGO-TEPA-Pb^{2+} and $Ab_{2,2}$-rGO-TEPA-Cu^{2+} hybrids. The antibodies are trapped on the surface of the rGO-TEPA-metal ion hybrids, indicating the successful fabrication of the Ab_2-rGO-TEPA-metal ion probes. To further confirm the successful preparation of the designed probes, UV–vis spectroscopy was employed. As shown in Figs. 2F and 3D, one adsorption peak at 550 nm was observed for the rGO-TEPA-metal ion hybrids (curve a). After the immobilization of Ab_2, a new absorption at 276 nm was observed (curve c), attributed to the adsorption peak from the Ab_2 itself (curve b) (Ma et al., 2015).

3.3. Characterization of the electrochemical immunosensor

To further monitor the successful formation of rGO-TEPA-metal ion hybrids, a series of delicate electrochemical measurements was conducted to characterise the immunosensor. As shown in Fig. 4A, no peak was observed for the rGO-TEPA-modified electrode in 0.2 M HAc/NaAc (pH=4.5) (curve a), but the rGO-TEPA-Pb^{2+}-modified electrode generated an obvious peak at −0.5 V in HAc/NaAc (curve b), resulting from the redox reaction of Pb^{2+}, which suggests that the Pb^{2+} ions were successfully adsorbed onto the rGO-TEPA. The DPV response on the rGO-TEPA-Cu^{2+}-modified electrode can be observed in Fig. 4B, with the electrode modified by rGO-TEPA-Cu^{2+} yielding one well-

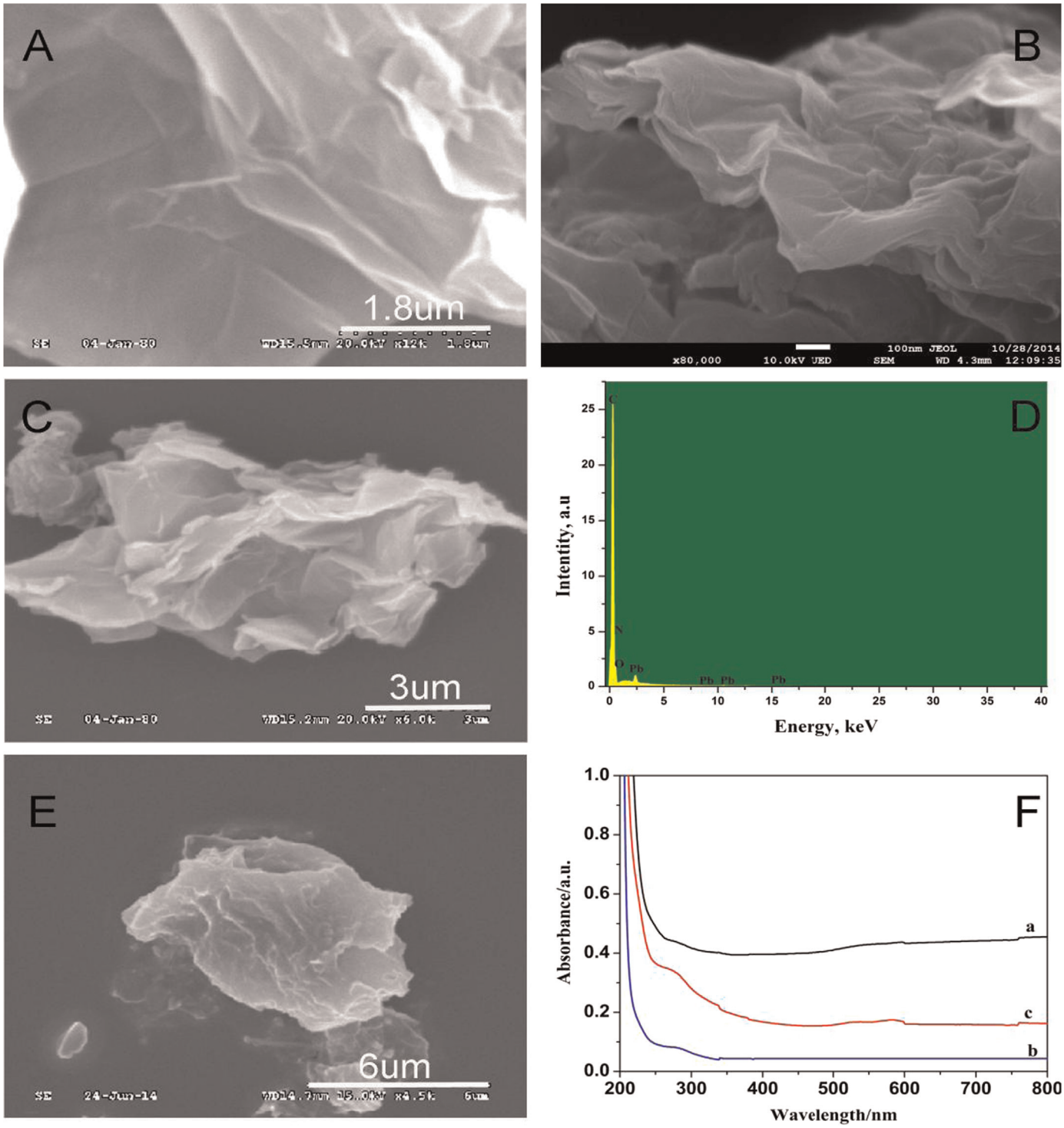

Fig. 2. SEM (A) and FE-SEM images (B) of rGO-TEPA, SEM image of (C) rGO-TEPA-Pb^{2+}, (D) EDS of rGO-TEPA-Pb^{2+}, SEM image of (E) Ab2-rGO-TEPA-Pb2+ as well as (F) UV–vis absorption spectra: rGO-TEPA-Pb^{2+} label (curve a), anti-hsCRP Ab2 (curve b), anti-hsCRP Ab2-rGO-TEPA-Pb^{2+} (curve c).

defined peak at approximately 0 V (curve b) compared to the rGO-TEPA-modified electrode (curve a), indicating that Cu^{2+} ions were also successively adsorbed onto the rGO-TEPA. Fig. 4C shows that the peaks of rGO-TEPA-Pb^{2+} and rGO-TEPA-Cu^{2+} are easily distinguishable due to their potential difference. Thus, the detection of hsCRP and sCD40L is possible based on the positions of the corresponding peaks.

The strong dual-signal amplification of the immunosensor signal by the Au@BSA and rGO-TEPA-metal ion labels is demonstrated in Fig. 4D. The principle of the analysis is displayed below

$$M^{n+} + n^{e-} \rightarrow M \quad (1)$$

$$M \rightarrow M^{n+} + n^{e-} \quad (2)$$

In the deposition step, Pb2+ and Cu2+ could be reduced to metallic Pb and Cu (Xu et al., 2014). Afterwards, the Pb^{2+} and Cu^{2+} could be oxidized and released in the stripping step, which generates the electrochemical signal (Liu et al., 2013). Compared with Pb^{2+}-Ab_2/hsCRP/Ab_1/GCE (curve a, Pb^{2+} ion bound directly with Ab_2 and used as the label), the immunosensor signals of

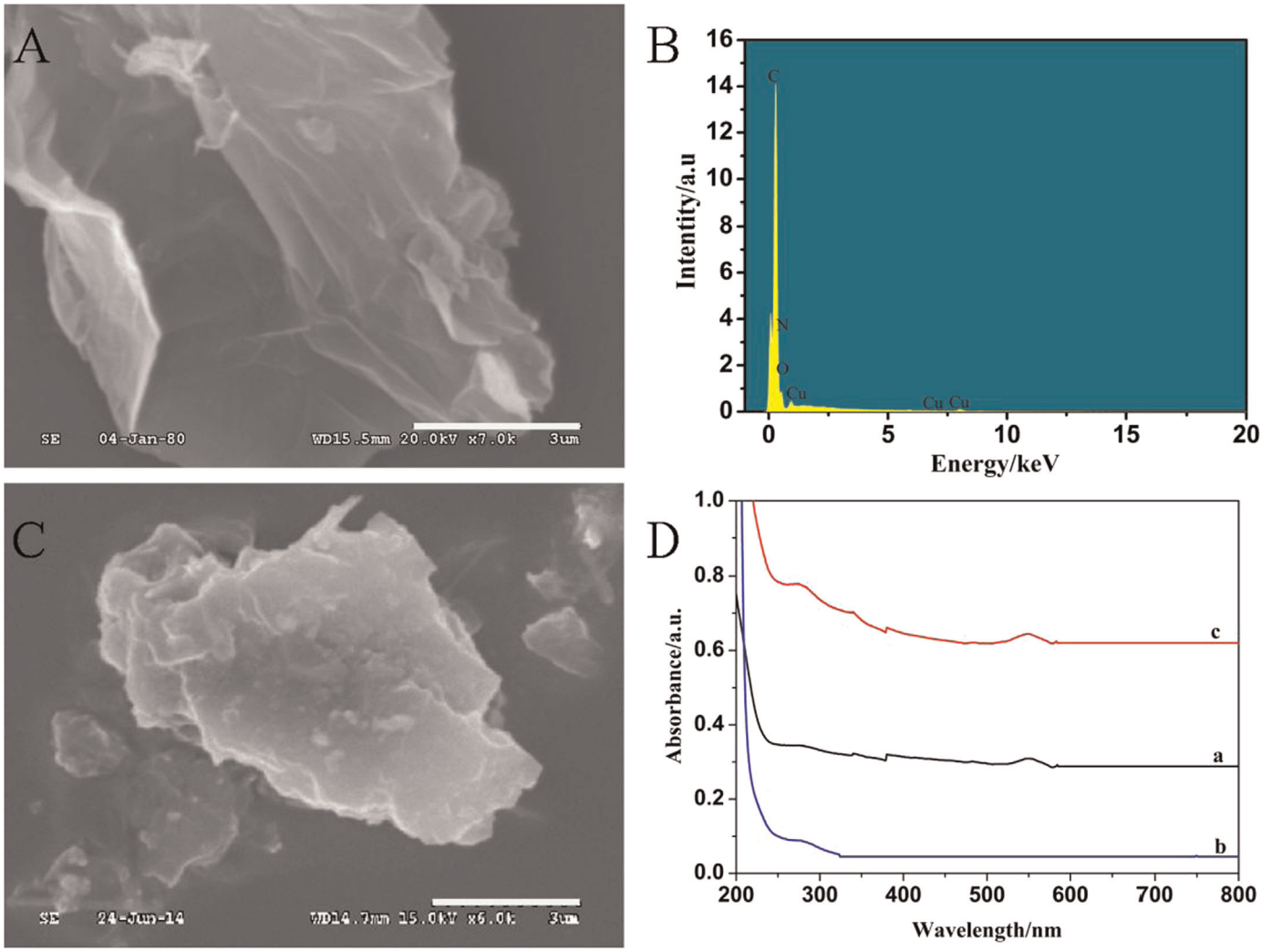

Fig. 3. SEM image of (A) rGO-TEPA-Cu^{2+}, (B) EDS of rGO-TEPA-Cu^{2+}, SEM image of (C) Ab2-rGO-TEPA-Cu^{2+} as well as (D) UV–vis absorption spectra: rGO-TEPA-Cu^{2+} label (curve a), anti-sCD40L Ab2 (curve b), anti-sCD40L Ab2- rGO-TEPA-Cu^{2+} (curve c).

Pb^{2+}-Ab_2/hsCRP/Ab_1/Au@BSA/GCE (curve b) and Pb^{2+}-rGO-TEPA-Ab_2/hsCRP/Ab_1/Au@BSA/GCE (curve c) are increased 12.8-fold and 24.6-fold, respectively. The result might be attributed to combining the advantages of the excellent conductivity of Au@BSA and rGO-TEPA with the increase in metal ions on the immunosensor surface.

As shown in Fig. 4E, CV experiments were performed to monitor the modification procedure of the electrodes in a 5 mM $K_3[Fe(CN)_6]/K_4[Fe(CN)_6]$ solution. A pair of the typical reversible redox peaks of ferricyanide ions can be observed on the bare GCE (curve a). After the electrode was modified with Au@BSA, the peak current of the CV increased (curve b) because the excellent electrical conductivity of Au@BSA facilitates electron transfer (Cao et al., 2015; Ma et al., 2015). When the modified electrode was incubated with GA (curve c), the peak current decreased owing to the poor conductivity of GA. When the modified electrode was immobilised with a mixture of capture anti-hsCRP and anti-sCD40L (curve c), the peak current obviously decreased owing to its ability to hinder the electron transfer of proteins. Afterwards, the peak current sharply declined further after the immunosensor was blocked with BSA (curve e) due to the formation of a hydrophobic protein layer. Thereafter, the resultant immunosensor reacted with analytes, and the peak current further decreased (curve d) because the formation of an immunocomplex layer blocked the electron transfer.

Electrochemical impedance spectroscopy (EIS) has been proven to be one of the most powerful tools for probing the features of surface-modified electrodes (Zhang et al., 2014c). Therefore, to further illustrate that all of the fabrication steps were effective, the electrochemical behaviors were characterised by electrochemical impedance spectroscopy using 5 mM $K_3[Fe(CN)_6]/K_4[Fe(CN)_6]$ solution. It is well known that the semicircle diameter in EIS is equal to the electron transfer resistance (R_{et}), and that the linear part of the curve at low frequency represents the diffusion process. As shown in Fig. 4F, when Au@BSA was modified onto the electrode, the resistance decreased (curve b) compared with the bare GCE (curve a), indicating that the Au@BSA accelerated the electron transfer of the electrode. When the cross-linking agent GA was modified onto the electrode, the resistance increased (curve c) slightly, indicating that the cross-linking agent hindered the electron transfer between the electrode and the solution. Afterwards, a large semicircle diameter was seen when the Ab_1 was dropped onto the electrode (curve d), implying that the Ab_1 was successively immobilised onto the electrode. This larger diameter might be attributed to an insulating layer of proteins hindering the diffusion of electrons between the electrolyte and the electrode surface (Yang et al., 2014). After the electrode was coated with BSA (curve e) and the analytes (curve f), the R_{et} increased dramatically due to proteins that were not electroactive hindering electron transfer. Subsequently, with Ab_2-rGO-TEPA-metal ion probes

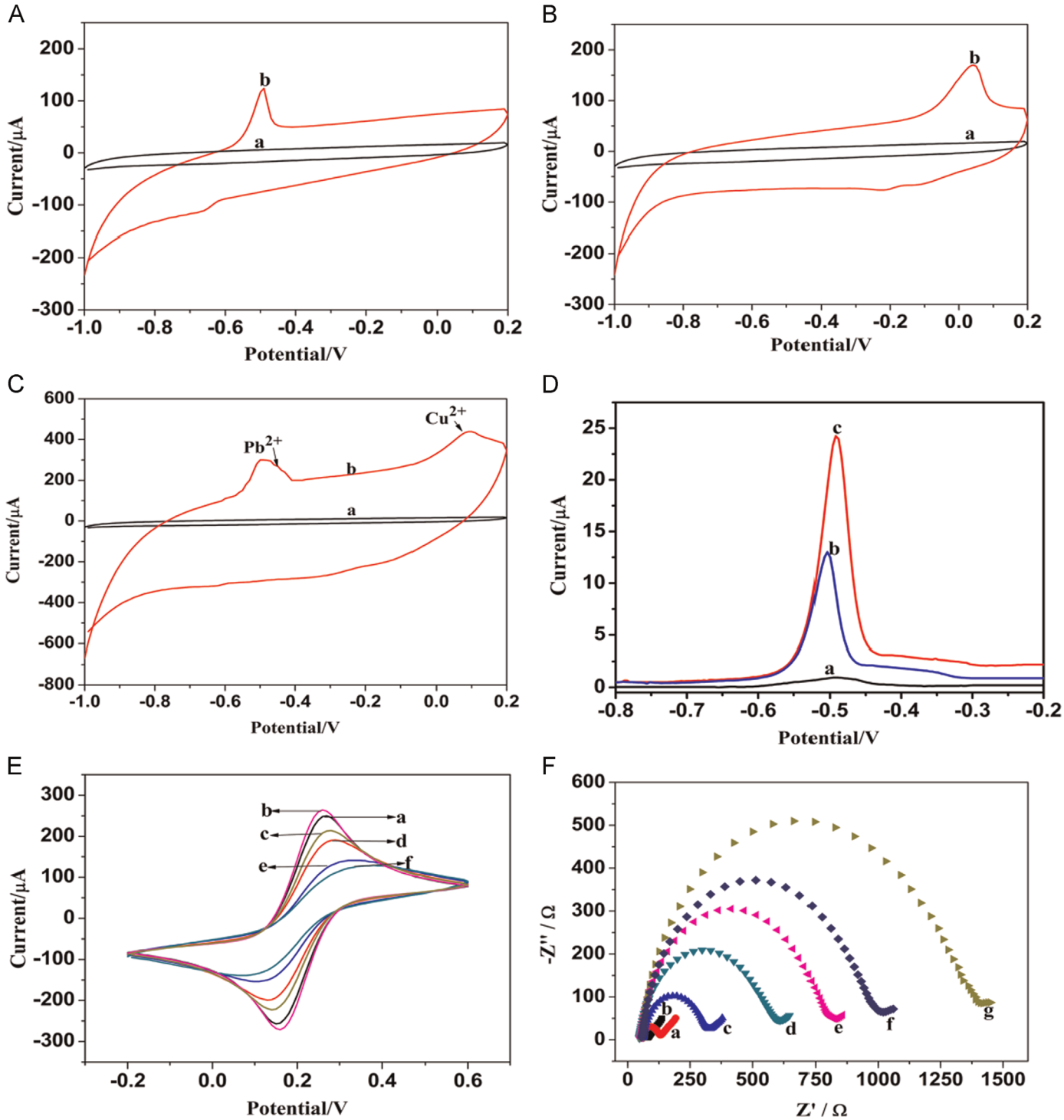

Fig. 4. (A) CV responses of (a) 2 mg mL^{-1} rGO-TEPA and (b) 2 mg mL^{-1} rGO-TEPA-Pb^{2+}; (B) (a) 2 mg mL^{-1} rGO-TEPA and (b) 2 mg mL^{-1} rGO-TEPA-Cu^{2+}; (C) (a) 2 mg mL^{-1} rGO-TEPA and (b) 2 mg mL^{-1} rGO-TEPA-Pb^{2+} and 2 mg mL$-^{1}$ rGO-TEPA-Cu^{2+} in 0.2 M pH 4.5 NaAc/HAc buffer solution; (D) DPV responses of the immunosensor using different immunocomplexes at an hsCRP concentration of 1 ng mL^{-1}: (a) Bare GCE Ab1/hsCRP/Ab2-rGO-TEPA-Pb^{2+}; (b) GCE/Au@BSA/GA/Ab1/hsCRP/Ab2-Pb^{2+} (c) GCE/Au@BSA/GA/Ab1/hsCRP/Ab2-rGO-TEPA-Pb^{2+}. (E) CV characterization of electrodes at various stages of modification in a 5 mM $[Fe(CN)_6]^{3-/4-}$ solution containing 0.1 M KCl: (a) bare GCE, (b) Au@BSA/GCE, (c) GA/Au@BSA/GCE (c) Ab1S/GA/Au@BSA/GCE, (d) BSA/Ab1S/GA/Au@BSA/GCE, (e) AgS/BSA/Ab1S /GA/Au@GS/GCE; (F) EIS for each immobilization step in 5 mM [Fe(CN)6] containing 0.1 M KCl solution: (a) bare GCE, (b) Au@BSA/GCE, (c) GA/Au@BSA/GCE (c) Ab1S/GA/Au@BSA/GCE, (d) BSA/Ab1S/GA/Au@BSA/GCE, (e) AgS/BSA/Ab1S/GA/Au@BSA/GCE and (f) Ab2-rGO-TEPA-metal ion/AgS/BSA/Ab1S/GA/Au@BSA/GCE, in 5 mM [Fe(CN)6] containing 0.1 M KCl solution.

(anti-hsCRP-rGO-TEPA-Pb^{2+} and anti-sCD40L-rGO-TEPA-Cu^{2+}) immobilised onto the electrode, the resistance increased (curve g), indicating that the immunosensor had indeed been successfully fabricated (Zhang et al., 2014c).

3.4. Optimization of conditions for electrochemical detection

The optimum conditions (the concentrations of Au@BSA, pH and incubation time) were determined, as shown in Fig. 5. A detailed description can be found in the Supplementary information.

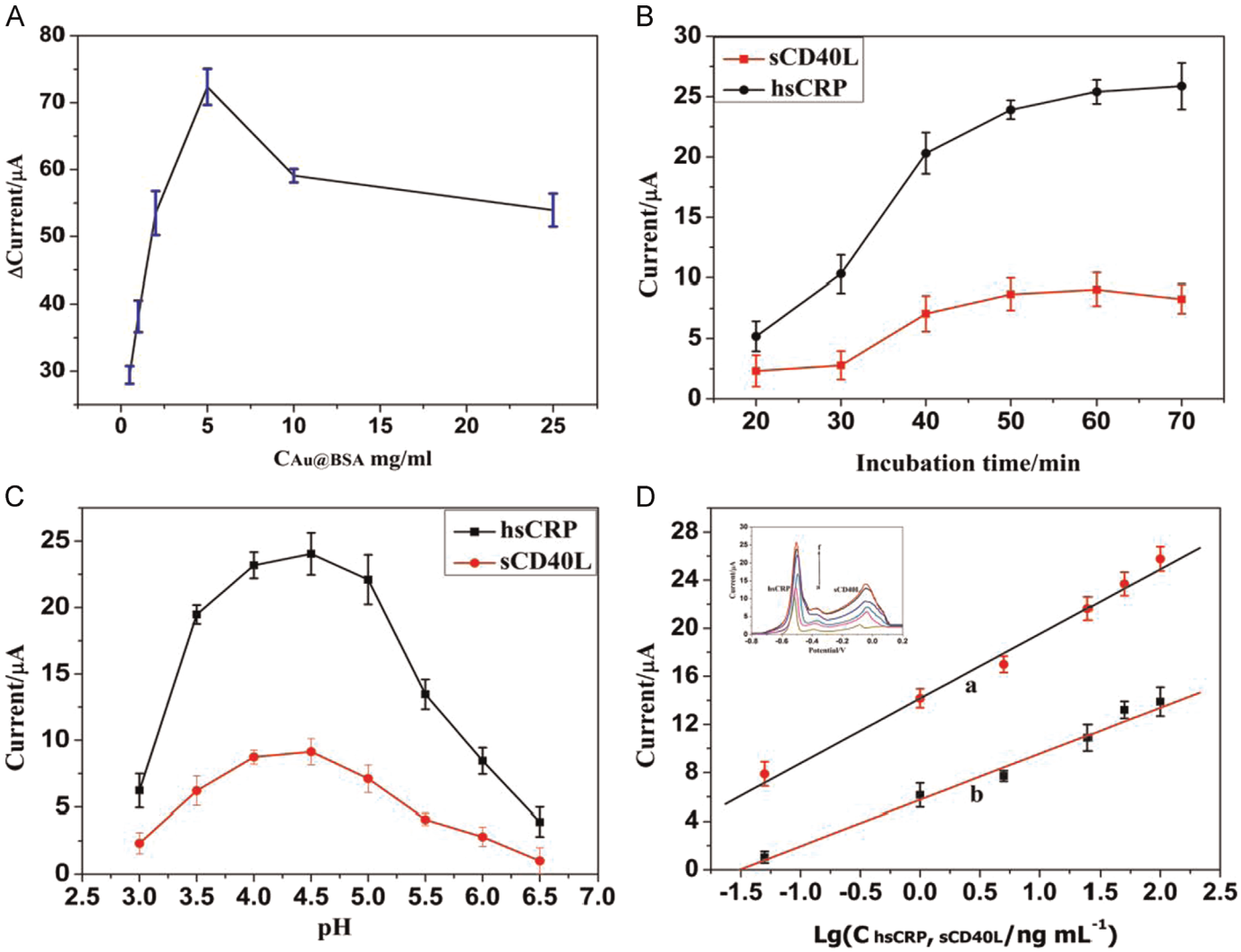

Fig. 5. Effects of the concentration of Au@BSA (A), pH of the detection solution (B), and incubation time (C) on the immunosensor. (D) Calibration curves of the immunosensor for different concentrations of hsCRP and sCD40L (curve a: hsCRP, curve b: sCD40L) ($n=3$). Inset of (D) shows the DPV signals of the immunosensor in corresponding concentrations of hsCRP and sCD40L.

3.5. Analytical performance of the multiplexed immunoassay

Under the optimal assay conditions, the performance of the proposed immunosensor was evaluated with different concentrations of hsCRP and sCD40L in the incubation mixture. The current peaks at −0.5 and 0 V were simultaneously recorded by DPV due to the oxidation of lead and copper, respectively. As indicated in the inset of Fig. 5D, the peak currents of the Pb^{2+} and Cu^{2+} increased with the increasing concentrations of hsCRP and sCD40L in the sample solutions; a sample solution containing 3 mL of the blank serum sample was analyzed at the same time. The calibration plots show a good linear relationship between the peak current and the logarithmic value of the analyte concentration, as shown in Fig. 5D. For hsCRP (curve a), the linear regression equation was I (μA)=14.159+5.378 Lg C_{hsCRP} (ng mL^{-1}) in the range of 0.05 ng mL^{-1} to 100 ng mL^{-1} with a correlation coefficient of 0.993. For sCD40L (curve b), the linear regression equation was I (μA)=5.757+3.813 Lg C_{sCD40L} (ng mL^{-1}) in the range of 0.05 ng mL^{-1} to 100 ng mL^{-1}, with a correlation coefficient of 0.991. The detection limits for hsCRP and sCD40L were estimated to be 16.7 pg mL^{-1} and 13.1 pg mL^{-1} at a signal-to-noise ratio of 3σ (where σ is the standard deviation of the blank, $n=6$), respectively, which are lower than those of other reported studies. A comparison of the linear ranges and detection limits between the proposed immunosensor and some other studies is provided in Table S4, indicating that the proposed immunosensor has relatively low detection limits, which might be attributed to the significant loading of metal ions onto the immunosensor surface, which greatly amplifies the peak signals. The detection limits of the immunosensor can meet the demands of practical tests.

3.6. Repeatability, specificity and stability of the multiplexed immunoassay

To evaluate the reproducibility of the immunosensor, the fabricated electrodes were assessed by the intra- and interassay relative standard derivations (RSDs), as shown in Fig. 6A and Table S5 in the Supplementary information. The intra-assay precision of the developed immunoassay was calculated by detecting three samples containing 0.05, 1, and 50 ng mL^{-1} of hsCRP and sCD40L, respectively. Each sample was measured five times using five immunosensors prepared in parallel. For different concentrations of hsCRP and sCD40L, the intra-assay RSD values were less than 4.77% and 3.79%, respectively. The interassay precision was estimated by measuring one sample with three immunosensors independently made at the same GCE. As observed in Table S5, the RSD values were less than 5.04% and 4.08% for different concentrations of hsCRP and sCD40L, respectively. These results

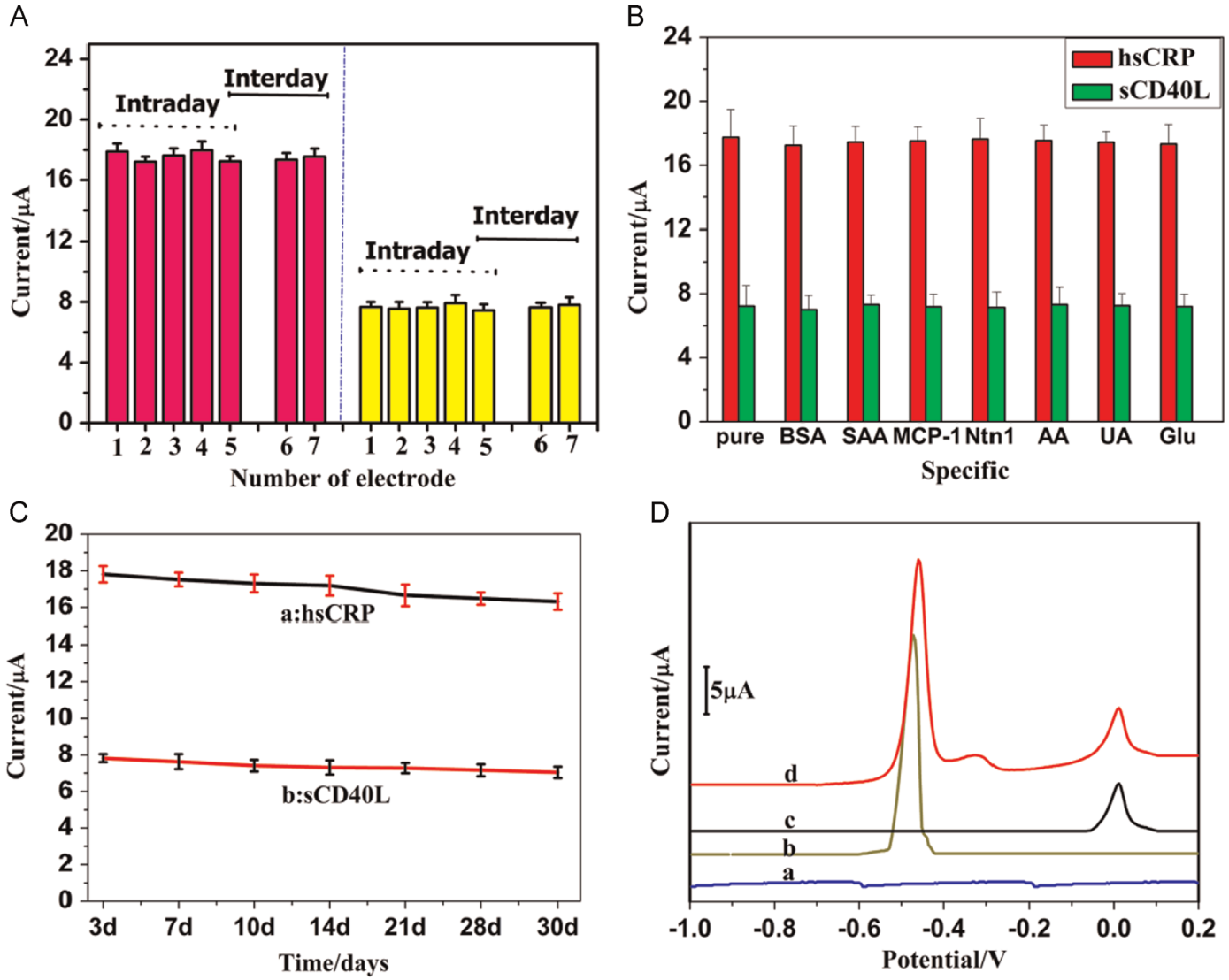

Fig. 6. (A) Reproducibility of 7 different electrodes modified with 1 ng mL^{-1} of hsCRP (red) and sCD40L (yellow). (B) Specificity of the immunosensor to 1 ng mL^{-1} hsCRP and sCD40L, 1 ng mL^{-1} hsCRP and sCD40L+50 ng mL^{-1} BSA, 1 ng mL^{-1} hsCRP and sCD40L+50 ng mL^{-1} SAA, 1 ng mL^{-1} hsCRP and sCD40L+50 ng mL^{-1} MCP-1, 1 ng mL^{-1} hsCRP and sCD40L+50 ng mL^{-1} Ntn1, 1 ng mL^{-1} hsCRP and sCD40L+50 ng mL^{-1} AA, 1 ng mL^{-1} hsCRP and sCD40L+50 ng mL^{-1} UA, 1 ng mL^{-1} hsCRP and sCD40L+50 ng mL^{-1} Glu. (C) Stability of the immunosensor in the presence of 1 ng mL^{-1} hsCRP and sCD40L, where $n=6$ for each point. (D) Signals for the investigation of cross-reactivity of the immunosensor with different analytes in the sandwich immunoassay: (a) 0 ng mL^{-1} hsCRP and sCD40L; (b) 1 ng mL^{-1} hsCRP; (c) 1 ng mL^{-1} sCD40L; (d) 1 ng mL^{-1} hsCRP and sCD40L. (For interpretation of the references to color in this figure legend, the reader is referred to the web version of this article.)

indicate that the proposed multianalyte immunoassay possesses acceptable precision and reproducibility.

Specificity plays an important role in the analysis of biological samples. Other proteins such as bovine serum albumin (BSA), SAA, monocyte chemoattractant protein-1 (MCP-1), Ntn1, ascorbic acid (AA), urea acid (UA) and D-(+)-glucose (Glu) were used as possible interferences to evaluate the specificity of the proposed immunosensor. Then, 1 ng mL^{-1} hsCRP and sCD40L was mixed with 50 ng mL^{-1} of BSA, SAA, MCP-1, Ntn1, AA, UA and Glu. The responses of the immunosensors were measured and are shown in Fig. 6B. Compared with the current response obtained from 1 ng mL^{-1} hsCRP and sCD40L, the peak currents showed minimal difference from the incubation solution containing interfering agents, which indicates that the specificity of the immunosensor based on the specific antigen–antibody immunoreaction was acceptable.

The stability of the immunosensor is also a key factor in its development and application. The immunosensor was stored at 4 °C when it was not in use, and after 30 days of storage, it retained 91.63% and 90.02% of its initial response to 1 ng mL^{-1} hsCRP and sCD40L, respectively (Fig. 6C). These results indicate the good stability of the proposed immunosensor, which might be ascribed to the good biocompatibility of the Au@BSA and rGO-TEPA, enabling them to retain the bioactivity of the protein.

3.7. Evaluation of cross-reactivity

An excellent immunosensor for simultaneous multianalyte detection must exclude cross-reactivity between analytes and nonspecific antibodies. Therefore, the immunosensor was used to detect hsCRP, sCD40L and a mixture of the two analytes. The amperometric responses were measured by differential pulse voltammetry (DPV). As shown in Fig. 6D and Fig. S2 (Supplementary information), there was one well-defined peak at – 0.5 V (vs. Ag/AgCl), which corresponds to hsCRP (Fig. S2A). Using the described method, a series of different concentrations of hsCRP was measured in the absence of sCD40L, and the results show that the peak current was linear to the hsCRP concentration in the

range of 0.05 to 100 ng mL^{-1} (inset of Fig. S2A). The regression equation was I_1 (μA)=16.195+7.004 Lg C_{hsCRP} (ng mL^{-1}), with a correlation coefficient of 0.993. Peaks were similarly obtained at 0 V when a series of different concentrations of sCD40L was measured in the absence of hsCRP, and the results show that the peak current was linear to the sCD40L concentration in the range of 0.05 to 100 ng mL^{-1} (inset of Fig. S2B). The regression equation was I_2 (μA)=10.576+4.380 Lg C_{sCD40L} (ng mL^{-1}), with a correlation coefficient of 0.996. When the immunosensor was incubated with different concentrations of one antigen in the presence of the other one, the results were as shown in Fig. 5D (inset). From these figures, we see that the detection of multianalytes would not cause interference with each other and that the cross-reactivity between the two analytes was negligible.

3.8. Application in analysis of human serum samples

To investigate the analytical reliability and application potential of the proposed method, the assay results of three human serum samples from a local hospital using the proposed method were compared with reference values obtained by the commercial enzyme-linked immunosorbent assay (ELISA) method. It can be observed from Table S1 that the relative errors between the two methods ranged from −3.7% to 4.4%, indicating acceptable accuracy. The results show that the developed immunosensor could be satisfactorily applied to the determination of hsCRP and sCD40L in serum samples.

To further investigate the potential application of the immunosensor for practical analysis, the immunosensor was used to test the recoveries of three concentrations of hsCRP and sCD40L in human serum samples. Three concentrations of hsCRP (0.1, 50 and 100 ng mL^{-1}) and sCD40L (0.1, 5 and 25 ng mL^{-1}) spiked human serum samples were prepared by standard addition methods. It can be observed from Table S2 that the recoveries of hsCRP were in the range of 105.26% to 109.79%, with relative standard deviations in the range of 2.73% to 4.21%. As observed in Table S3, the recoveries of sCD40L were in the range of 98.11% to 101.80%, with relative standard deviations in the range of 1.05% to 3.24%. The results show that the developed immunosensor might be preliminarily applied for the determination of hsCRP and sCD40L in real samples.

4. Conclusions

In this work, a novel simplified multiplexed electrochemical immunoassay for the simultaneous detection of hsCRP and sCD40L was developed using Au@BSA as a sensing platform and biofunctionalized rGO-TEPA as distinguishable signal probes for dual-signal amplification. The highlights of this work could be summarized as follows: (1) rGO-TEPA was used as a template for the adsorption of metal ions to further label antibodies for the first time. (2) The usage of rGO-TEPA as signal tag materials simplified the usual operation by excluding the amination process based on rGO-TEPA qualified with abundant amino groups. (3) This is the first report of the detection of hsCRP and sCD40L by an immunosensor in a single run. (4) The combined measurement may not only increase the sensitivity of the risk prediction but may also provide new cardiac markers to replace cardiac enzymes for the clinical diagnosis and risk evaluation of cardiovascular events. Significantly, the universal method demonstrated here opens up a new straightforward approach for the determination of other biomarkers. Based on our achievement in developing a probe-tagging strategy, we will attempt to apply it to a chip or array in future work to improve the assay throughput.

Acknowledgments

The research was financed by the National Natural Science Foundation of China (Nos. 81370403 and 21205146).

Appendix A. Supplementary material

Supplementary data associated with this article can be found in the online version at http://dx.doi.org/10.1016/j.bios.2015.04.088.

References

Apple, F.S., 2007. Clin. Chim. Acta 380 (1–2), 1–3, Discussion 245–246.
Babakhanian, A., Ehzari, H., Kaki, S., Hamidi, Z., 2015. Biosens. Bioelectron. 63, 490–498.
Bai, L., Yuan, R., Chai, Y., Zhuo, Y., Yuan, Y., Wang, Y., 2012. Biomaterials 33, 1090–1096.
Cao, H., Yang, D.-P., Ye, D., Zhang, X., Fang, X., Zhang, S., Liu, B., Kong, J., 2015. Biosens. Bioelectron 68, 329–335.
Dieset, I., Hope, S., Ueland, T., Bjella, T., Agartz, I., Melle, I., Aukrust, P., Rossberg, J.I., Andreassen, O.A., 2012. Schizophr. Res. 140, 169–174.
Erturan, I., Koroglu, B.K., Adiloglu, A., Ceyhan, A.M., Akkaya, V.B., Tamer, N., Basak, P. Y., Korkmaz, S., Ersoy, I.H., Kilinc, O., 2014. Int. J. Dermatol. 53, 503–509.
Fakanya, W., Tothill, I., 2014. Biosensors 4, 340–357.
Feng, L.N., Bian, Z.P., Peng, J., Jiang, F., Yang, G.H., Zhu, Y.D., Yang, D., Jiang, L.P., Zhu, J. J., 2012a. Anal. Chem. 84, 7810–7815.
Feng, L.N., Peng, J., Zhu, Y.D., Jiang, L.P., Zhu, J.J., 2012b. Chem. Commun. 48, 4474–4476.
Gibler, W.B., Cannon, C.P., Blomkalns, A.L., Char, D.M., Drew, B.J., Hollander, J.E., Jaffe, A.S., Jesse, R.L., Newby, L.K., Ohman, E.M., Peterson, E.D., Pollack, C.V., 2005. Ann. Emerg. Med. 46, 185–197.
Guldiken, S., Guldiken, B., Demir, M., Kabayel, L., Ozkan, H., Turgut, N., Hunkar, R., Kat, S., 2011. J. Headache Pain 12, 355–360.
Guo, A., Li, Y., Cao, W., Meng, X., Wu, D., Wei, Q., Du, B., 2015. Biosens. Bioelectron. 63, 39–46.
Jia, X., Chen, X., Han, J., Ma, J., Ma, Z., 2014. Biosens. Bioelectron. 53, 65–70.
Li, W., Li, L., Ge, S., Song, X., Ge, L., Yan, M., Yu, J., 2014. Biosens. Bioelectron. 56, 167–173.
Li, W., Li, L., Li, M., Yu, J., Ge, S., Yan, M., Song, X., 2013. Chem. Commun. 49, 9540–9542.
Liu, H., Xu, S., He, Z., Deng, A., Zhu, J.J., 2013. Anal. Chem. 85, 3385–3392.
Liu, Y., Kwa, T., Revzin, A., 2012. Biomaterials 33, 7347–7355.
Ma, C., Li, W., Kong, Q., Yang, H., Bian, Z., Song, X., Yu, J., Yan, M., 2015. Biosens. Bioelectron. 63, 7–13.
Qu, Q.X., Huang, Q., Xu, J., Duan, L.T., Zhu, Y.B., Zhang, X.G., 2013. Oncol. Res. 20, 383–392.
Unek, I.T., Bayraktar, F., Solmaz, D., Ellidokuz, H., Sisman, A.R., Yuksel, F., Yesil, S., 2010. Clin. Med. Res. 8, 89–95.
Vashist, S.K., Marion Schneider, E., Zengerle, R., von Stetten, F., Luong, J.H., 2015. Biosens. Bioelectron. 66, 169–176.
Wang, Z., Liu, N., Ma, Z., 2014. Biosens. Bioelectron. 53, 324–329.
Willcox, B.J., Abbott, R.D., Yano, K., Rodriguez, B.L., Willcox, D.C., Curb, J.D., 2004. Expert Rev. Neurother. 4, 507–518.
Wu, D., Guo, A., Guo, Z., Xie, L., Wei, Q., Du, B., 2014. Biosens. Bioelectron. 54, 634–639.
Wu, D., Guo, Z., Liu, Y., Guo, A., Lou, W., Fan, D., Wei, Q., 2015. Talanta 134, 305–309.
Xu, T., Jia, X., Chen, X., Ma, Z., 2014. Biosens. Bioelectron. 56, 174–179.
Yang, F., Han, J., Zhuo, Y., Yang, Z., Chai, Y., Yuan, R., 2014. Biosens. Bioelectron. 55, 360–365.
Zhang, B., Chen, M., Yang, H., Wu, T., Song, C., Guo, R., 2014a. Neurosci. Lett. 567, 6–10.
Zhang, S., Du, B., Li, H., Xin, X., Ma, H., Wu, D., Yan, L., Wei, Q., 2014b. Biosens. Bioelectron. 52, 225–231.
Zhang, X., Li, F., Wei, Q., Du, B., Wu, D., Li, H., 2014c. Sens. Actuators B: Chem. 194, 64–70.
Zhao, L., Wei, Q., Wu, H., Dou, J., Li, H., 2014. Biosens. Bioelectron. 59C, 75–80.